

University of Massachusetts Medical School  
**eScholarship@UMMS**

---

[Open Access Articles](#)

[Open Access Publications by UMMS Authors](#)

---

2014-08-14


## A deterministic model predicts the properties of stochastic calcium oscillations in airway smooth muscle cells

Pengxing Cao  
*University of Auckland*

*Et al.*

Let us know how access to this document benefits you.

Follow this and additional works at: <https://escholarship.umassmed.edu/oapubs>

 Part of the [Biostatistics Commons](#), [Cellular and Molecular Physiology Commons](#), [Computational Biology Commons](#), and the [Statistical Models Commons](#)

---

### Repository Citation

Cao P, Tan X, Donovan G, Sanderson MJ, Sneyd J. (2014). A deterministic model predicts the properties of stochastic calcium oscillations in airway smooth muscle cells. Open Access Articles. <https://doi.org/10.1371/journal.pcbi.1003783>. Retrieved from <https://escholarship.umassmed.edu/oapubs/2463>

Creative Commons License



This work is licensed under a [Creative Commons Attribution 4.0 License](#).

This material is brought to you by eScholarship@UMMS. It has been accepted for inclusion in Open Access Articles by an authorized administrator of eScholarship@UMMS. For more information, please contact [Lisa.Palmer@umassmed.edu](mailto:Lisa.Palmer@umassmed.edu).



# A Deterministic Model Predicts the Properties of Stochastic Calcium Oscillations in Airway Smooth Muscle Cells

Pengxing Cao<sup>1</sup>, Xiahui Tan<sup>2</sup>, Graham Donovan<sup>1</sup>, Michael J. Sanderson<sup>2</sup>, James Sneyd<sup>1\*</sup>

<sup>1</sup> Department of Mathematics, University of Auckland, Auckland, New Zealand, <sup>2</sup> Department of Microbiology and Physiological Systems, University of Massachusetts Medical School, Worcester, Massachusetts, United States of America

## Abstract

The inositol trisphosphate receptor (IP<sub>3</sub>R) is one of the most important cellular components responsible for oscillations in the cytoplasmic calcium concentration. Over the past decade, two major questions about the IP<sub>3</sub>R have arisen. Firstly, how best should the IP<sub>3</sub>R be modeled? In other words, what fundamental properties of the IP<sub>3</sub>R allow it to perform its function, and what are their quantitative properties? Secondly, although calcium oscillations are caused by the stochastic opening and closing of small numbers of IP<sub>3</sub>R, is it possible for a deterministic model to be a reliable predictor of calcium behavior? Here, we answer these two questions, using airway smooth muscle cells (ASMC) as a specific example. Firstly, we show that periodic calcium waves in ASMC, as well as the statistics of calcium puffs in other cell types, can be quantitatively reproduced by a two-state model of the IP<sub>3</sub>R, and thus the behavior of the IP<sub>3</sub>R is essentially determined by its modal structure. The structure within each mode is irrelevant for function. Secondly, we show that, although calcium waves in ASMC are generated by a stochastic mechanism, IP<sub>3</sub>R stochasticity is not essential for a qualitative prediction of how oscillation frequency depends on model parameters, and thus deterministic IP<sub>3</sub>R models demonstrate the same level of predictive capability as do stochastic models. We conclude that, firstly, calcium dynamics can be accurately modeled using simplified IP<sub>3</sub>R models, and, secondly, to obtain qualitative predictions of how oscillation frequency depends on parameters it is sufficient to use a deterministic model.

**Citation:** Cao P, Tan X, Donovan G, Sanderson MJ, Sneyd J (2014) A Deterministic Model Predicts the Properties of Stochastic Calcium Oscillations in Airway Smooth Muscle Cells. *PLoS Comput Biol* 10(8): e1003783. doi:10.1371/journal.pcbi.1003783

**Editor:** Andrew D. McCulloch, University of California, San Diego, United States of America

**Received:** April 6, 2014; **Accepted:** June 24, 2014; **Published:** August 14, 2014

**Copyright:** © 2014 Cao et al. This is an open-access article distributed under the terms of the Creative Commons Attribution License, which permits unrestricted use, distribution, and reproduction in any medium, provided the original author and source are credited.

**Data Availability:** The authors confirm that all data underlying the findings are fully available without restriction. All relevant data are within the paper and its Supporting Information files.

**Funding:** Funding for all authors came from National Heart Lung Blood Institute (USA) RO1 HL103405. <http://www.nhlbi.nih.gov/> The funders had no role in study design, data collection and analysis, decisions to publish, or preparation of the manuscript.

**Competing Interests:** The authors have declared that no competing interests exist.

\* Email: [sneyd@math.auckland.ac.nz](mailto:sneyd@math.auckland.ac.nz)

## Introduction

Oscillations in cytoplasmic calcium concentration ( $[Ca^{2+}]_i$ ), mediated by inositol trisphosphate receptors (IP<sub>3</sub>R; a calcium channel that releases calcium ions ( $Ca^{2+}$ ) from the endoplasmic or sarcoplasmic reticulum (ER or SR) in the presence of inositol trisphosphate (IP<sub>3</sub>)) play an important role in cellular function in many cell types. Hence, a thorough knowledge of the behavior of the IP<sub>3</sub>R is a necessary prerequisite for an understanding of intracellular  $Ca^{2+}$  oscillations and waves. Mathematical and computational models of the IP<sub>3</sub>R play a vital role in studies of  $Ca^{2+}$  dynamics. However, over the past decade, two major questions about IP<sub>3</sub>R models have arisen.

Firstly, how best should the IP<sub>3</sub>R be modeled? Models of the IP<sub>3</sub>R have a long history, beginning with the heuristic models of [1–3]. With the recent appearance of single-channel data from IP<sub>3</sub>R *in vivo* [4,5], a new generation of Markov IP<sub>3</sub>R models has recently appeared [6,7]. These models show that IP<sub>3</sub>R exist in different modes with different open probabilities. Within each mode there are multiple states, some open, some closed. Importantly, it was found [8] that time-dependent transitions between different modes

are crucial for reproducing  $Ca^{2+}$  puff data from [9]. However, it is not yet clear whether transitions between states within each mode are important, or whether all the important behaviors are captured simply by inter-mode transitions.

Secondly, why do deterministic models of the IP<sub>3</sub>R perform so well as predictive models? Deterministic models of the IP<sub>3</sub>R have proven to be useful predictive models in a range of cell types. For example, IP<sub>3</sub>R-based models have been developed to study  $Ca^{2+}$  oscillations in airway smooth muscle cells (ASMC) [10–13], and these models have made predictions which have been confirmed experimentally. This shows the usefulness of such models in advancing our understanding of how intracellular  $Ca^{2+}$  oscillations and waves are initiated and controlled in ASMC. However, these models are deterministic models which assume infinitely many IP<sub>3</sub>R per unit cell volume, an assumption that contradicts experimental findings in many cell types showing that  $Ca^{2+}$  puffs and spikes occur stochastically, and that intracellular  $Ca^{2+}$  waves and oscillations arise as an emergent property of fundamental stochastic events [9,14,15].

Here, we answer these two fundamental modeling questions using data and models from ASMC. Firstly, we show that a simple

### Author Summary

The inositol trisphosphate receptor (IP<sub>3</sub>R) is one of the most important cellular components responsible for calcium oscillations. Over the past decade, two major questions about the IP<sub>3</sub>R have arisen. Firstly, what fundamental properties of the IP<sub>3</sub>R allow it to perform its function? Secondly, although calcium oscillations are caused by the stochastic properties of small numbers of IP<sub>3</sub>R is it possible for a deterministic model to be a reliable predictor of calcium dynamics? Using airway smooth muscle cells as an example, we show that calcium dynamics can be accurately modeled using simplified IP<sub>3</sub>R models, and, secondly, that deterministic models are qualitatively accurate predictors of calcium dynamics. These results are important for the study of calcium dynamics in many cell types.

model of the IP<sub>3</sub>R, involving only two states with time-dependent transitions, suffices to generate correct dynamics of Ca<sup>2+</sup> puffs and oscillations. Secondly, we show that, although Ca<sup>2+</sup> oscillations in ASMC are generated by a stochastic mechanism, a deterministic model can make the same qualitative predictions as the analogous stochastic model, indicating that deterministic models, that require much less computational time and complexity, can be used to make reliable predictions. Although we work in the specific context of ASMC, our results are applicable to other cell types that exhibit similar Ca<sup>2+</sup> oscillations and waves.

### Results

#### A two-state model of the IP<sub>3</sub>R is sufficient to reproduce function

We have previously shown [8] that the statistics of Ca<sup>2+</sup> puffs in SH-SY5Y cells can be reproduced by a Markov model of the IP<sub>3</sub>R based on the steady-state data of [5] and the time-dependent data of [4]. In this model the IP<sub>3</sub>R can exist in 6 different states, grouped into two modes, which we call *Drive* and *Park* (see Fig. 1). The Drive mode (which contains 4 states; 1 open and 3 closed) has an average open probability of around 0.7, while the Park mode (which contains the remaining two states; 1 open and 1 closed) has an open probability close to zero. Transitions between states within each mode are independent of Ca<sup>2+</sup> and IP<sub>3</sub>; only the transitions between modes are ligand-dependent.

In our previous study on calcium puffs [8], we showed that, to reproduce the experimentally observed non-exponential interspike interval (ISI) distribution and coefficient of variation (CV) of ISI smaller than 1, the time-dependent intermodal transitions are crucial. Lack of time dependencies in the Siekmann model leads to exponential ISI distributions and CV = 1, which is not the case for calcium spikes in ASMC. Fig. 2A shows an example of Ca<sup>2+</sup> oscillations generated by 50 nM methacholine (MCh, an agonist that can induce the production of IP<sub>3</sub> by binding to a G protein-coupled receptor in the cell membrane) in ASMC. By gathering data from 14 cells in 5 mouse lung slices, we found that the standard deviation of the interspike interval (ISI) is approximately a linear function of the ISI mean, with a slope clearly between 0 and 1 (i.e. CV < 1), indicating that the spikes are generated by an inhomogeneous Poisson process (a slope of 1 would denote a pure Poisson process) (see Fig. 2B). This shows the necessity of inclusion of time-dependent transitions for mode-switching.

Using a quasi-steady-state approximation, and ignoring states with very low dwell times, it is possible to construct a simplified two-state version of the full six-state model (see *Materials and*

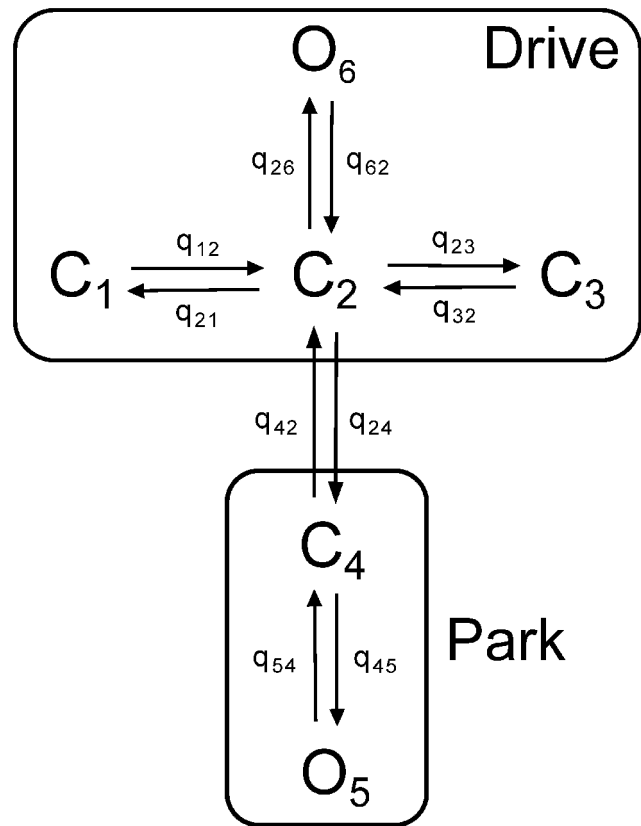


**Figure 1. The structure of the Siekmann IP<sub>3</sub>R model.** The IP<sub>3</sub>R model is comprised of two modes. One is the drive mode containing three closed states  $C_1$ ,  $C_2$ ,  $C_3$  and one open state  $O_6$ . The other is the park mode which includes one closed state  $C_4$  and one open state  $O_5$ .  $q_s$  are rates of state-transitions between two adjacent states and  $q_{42}$  and  $q_{24}$  are transitions between the two modes [7]. doi:10.1371/journal.pcbi.1003783.g001

*Methods*). In the simplified model the intramodal structure is ignored, and only the intermodal transitions have an effect on IP<sub>3</sub>R behavior. In Fig. 3 we compared the simplified IP<sub>3</sub>R model to the full six-state model. Both models have the same distribution of interspike interval, spike amplitude and spike duration. Moreover, by looking at a more detailed comparison between the two model results (Figs. 4A, C and E) and experimental data (Figs. 4B, D and F), we found the 2-state model not only can reproduce the behaviour of the 6-state model, but can also qualitatively reproduce experimental data. The average experimental ISI shows a clear decreasing trend as MCh concentration increases (although a saturation occurs in the data for high MCh), a trend that is mirrored by the model results as the IP<sub>3</sub> concentration increases. Unfortunately, since the exact relationship between MCh concentration and IP<sub>3</sub> concentration is uncertain, a quantitative comparison is not possible. In both model and experimental results, the average peak and duration of the oscillations are nearly independent of agonist concentration. The quantitative difference in spike duration between the model results and the data in Figs. 4E and F are most likely due to choice of calcium buffering parameters. For example, adding 3 or 5  $\mu\text{M}$  fast Ca<sup>2+</sup> buffer (see *Materials and Methods*) increases the average spike duration to 0.54 s or 0.7 s respectively, which are close to the levels shown in the data.

Thus, the intramodal structure of the six-state model is essentially unimportant, as the model behavior (in terms of the

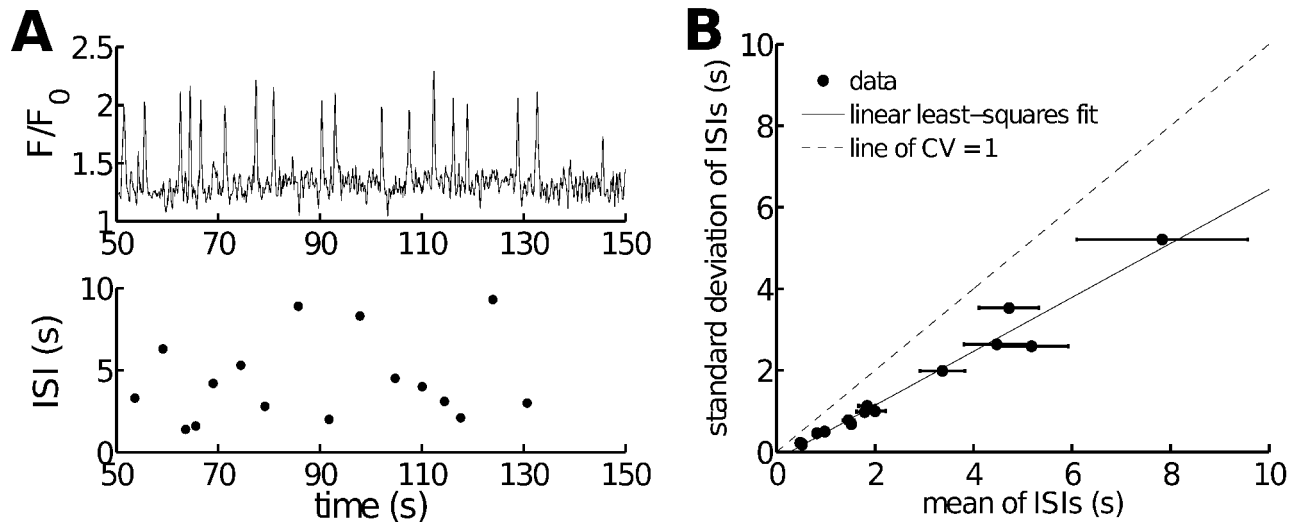


**Figure 2.  $\text{Ca}^{2+}$  oscillations in ASMC in lung slices are generated by a stochastic mechanism.** **A:** experimental  $\text{Ca}^{2+}$  spiking in ASMC in lung slices, stimulated with 50 nM MCh. In the upper panel we filter out baseline noise by using a low threshold of 1.42 (relative fluorescence intensity) and then choose samples with amplitude larger than 1.75. The ISI calculated from the upper panel is shown in the lower panel. **B:** relationship between the standard deviation and the mean of experimental ISIs. Data obtained from 14 ASMC in 5 mouse lung slices. The relationship is approximately linear with a slope of 0.66, which implies that an inhomogeneous Poisson process governs the generation of oscillations. The dashed line indicates where the coefficient of variation (CV) is 1 (as it is for a pure Poisson process). Variation in ISI is mainly caused by both use of different doses of MCh and different sensitivities of different cells to MCh. Error bars indicate the standard errors of the means (SEM). doi:10.1371/journal.pcbi.1003783.g002

statistics of puffs and oscillations) is governed almost entirely by the time dependence of the intermode transitions, particularly the time dependence of the rapid inhibition of the  $\text{IP}_3\text{R}$  by high  $[\text{Ca}^{2+}]_i$ , and the slow recovery from inhibition by  $\text{Ca}^{2+}$ . The multiple states within each mode are necessary to obtain an acceptable quantitative fit to single-channel data, but are nevertheless of limited importance for function. Hence, even when simulating microscopic events such as  $\text{Ca}^{2+}$  puffs it is sufficient to use a simpler, faster, two-state model, rather than a more complex six-

state model. In the following, we will use the 2-state  $\text{IP}_3\text{R}$  model to generate all the simulation results.

#### Prediction of stochastic $\text{Ca}^{2+}$ behavior by a deterministic model

Although the data (Fig. 2) show that  $\text{Ca}^{2+}$  oscillations in ASMC are generated by a stochastic process, not a deterministic one, we wish to know to what extent a deterministic model can be used to make qualitative (and experimentally testable) predictions. Our

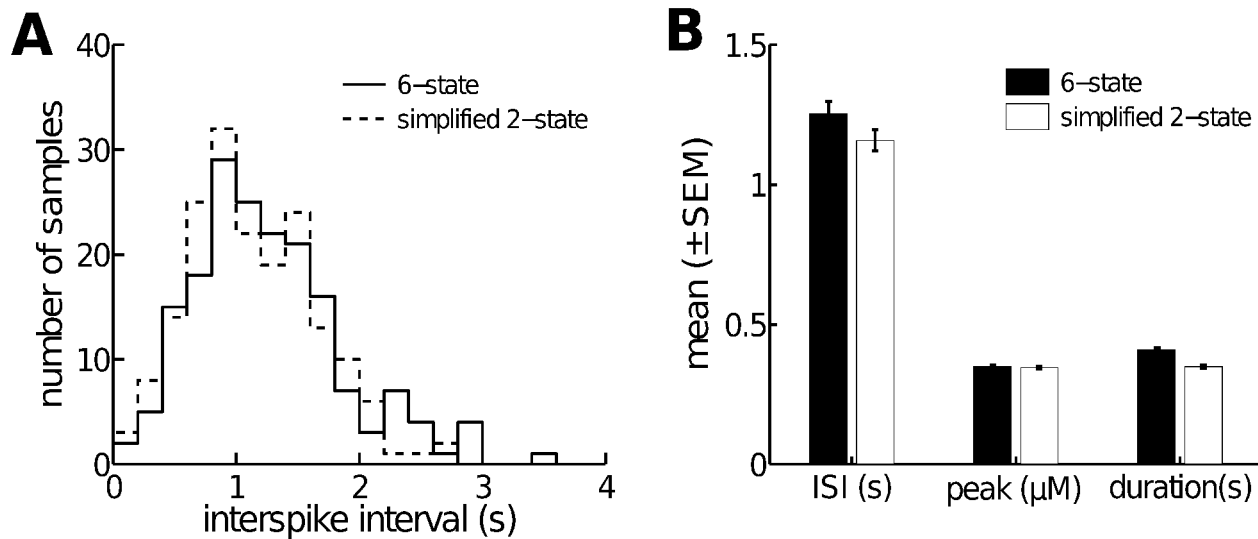


**Figure 3. A 2-state open/closed model quantitatively reproduces the 6-state  $\text{IP}_3\text{R}$  model.** **A:** histograms of interspike interval (ISI) distribution for both the 6-state and the simplified models. The ISI is defined to be the waiting time between successive spikes. Each histogram contain an equal number of samples (180). **B:** comparison of average ISI, average peak value of  $[\text{Ca}^{2+}]_i$  ( $c$  in the model) and average spike duration. All distributions were computed at a constant  $[\text{IP}_3] = 0.15 \mu\text{M}$ . doi:10.1371/journal.pcbi.1003783.g003

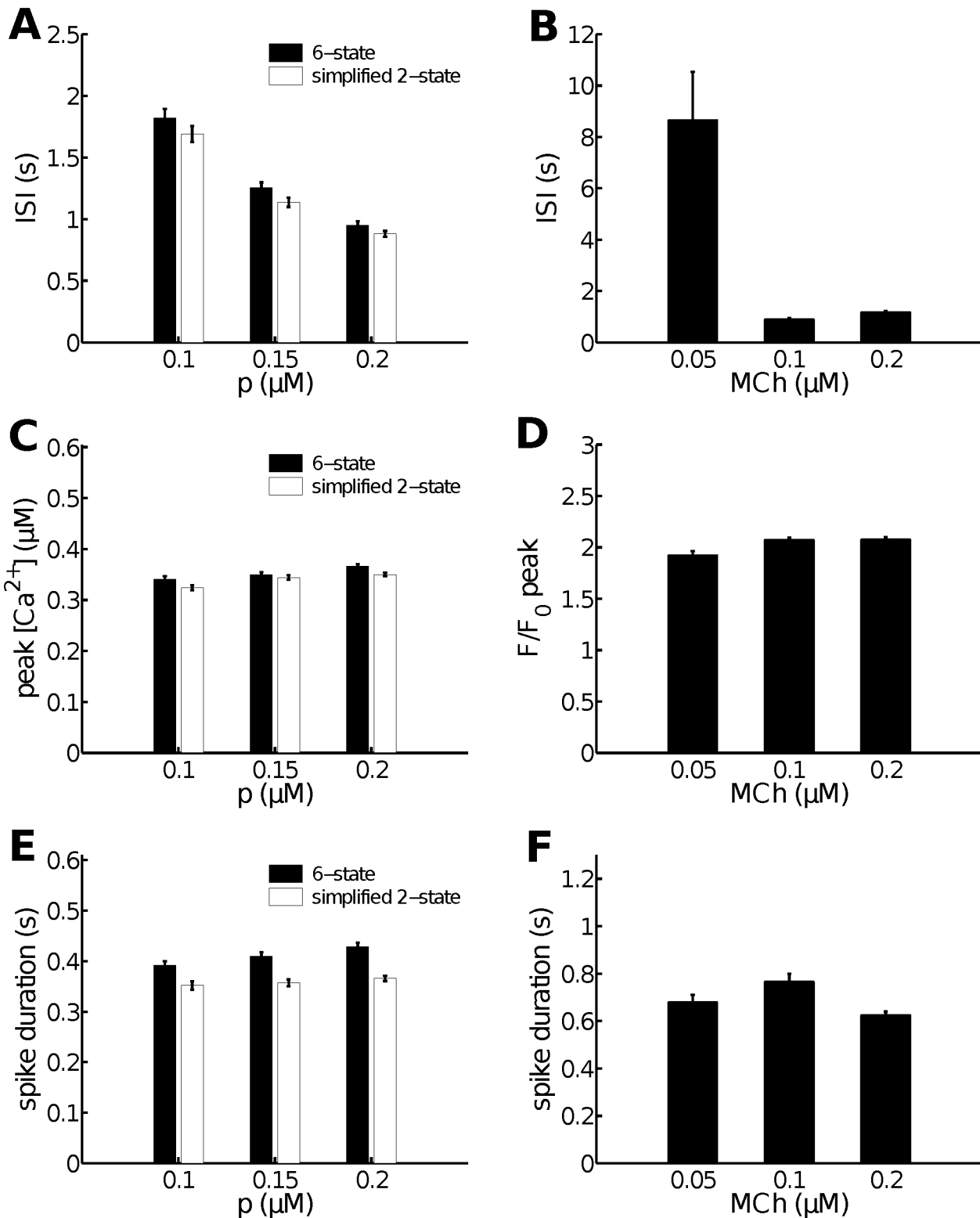


**Figure 4. More detailed comparisons between the 2-state and the 6-state  $\text{IP}_3\text{R}$  models, and a comparison to experimental data.** As a function of  $\text{IP}_3$  concentration ( $p$ ), the two models give the same ISI (A), peak  $[\text{Ca}^{2+}]_i$  (C) and spike duration (E). These results agree qualitatively with experimental data, as shown in panels B, D and F respectively. Quantitative comparisons are generally not possible as the relationship between  $\text{IP}_3$  concentration and agonist concentration is not known. Error bars represent mean  $\pm$  SEM. Data for each MCh concentration are obtained from at least three different cells from at least two different lung slices.  
doi:10.1371/journal.pcbi.1003783.g004

simplified 2-state Markov model of the IP<sub>3</sub>R can be converted to a deterministic model (see *Materials and Methods*). The result is a system of ordinary differential equations (ODEs) with four variables, which takes into account the increased [Ca<sup>2+</sup>]<sub>i</sub> at an open IP<sub>3</sub>R pore, as well as the increased [Ca<sup>2+</sup>]<sub>i</sub> within a cluster of IP<sub>3</sub>R; the four variables are the [Ca<sup>2+</sup>]<sub>i</sub> outside the IP<sub>3</sub>R cluster (*c*), the [Ca<sup>2+</sup>]<sub>i</sub> within the IP<sub>3</sub>R cluster (*c<sub>b</sub>*), the total intracellular Ca<sup>2+</sup> concentration (*c<sub>t</sub>*) and an IP<sub>3</sub>R gating variable (*h<sub>42</sub>*). We refer to the reduced 4D model as the deterministic model for all the results and analyses.

Note that there is no physical or geometric constraint enforcing a high local [Ca<sup>2+</sup>]<sub>i</sub>; in this case the spatial heterogeneity arises solely from the low diffusion coefficient of Ca<sup>2+</sup>. Our use of *c<sub>b</sub>* is merely a highly simplified way of introducing spatial heterogeneity of the Ca<sup>2+</sup> concentration. Since the IP<sub>3</sub>R can only “see” *c<sub>b</sub>* (as well as the Ca<sup>2+</sup> concentration right at the mouth of an open channel, which we denote by *c<sub>p</sub>*), but cannot be influenced directly by *c* (the experimentally observed Ca<sup>2+</sup> signal), our approach allows for the functional differentiation of the rapid local oscillatory Ca<sup>2+</sup> in the cluster, from the slower Ca<sup>2+</sup> signal in the cytoplasm, without the need for computationally intensive simulations of a partial differential equation model. Quantitative accuracy is thus sacrificed for computational convenience.

Calcium oscillations in the stochastic and deterministic models are shown in Fig. 5A. According to our previous results [8], the average value of *h<sub>42</sub>* over the cluster of IP<sub>3</sub>R primarily regulates the termination and regeneration of individual spikes. This can be seen in the stochastic model by projecting the solution on the *c<sub>b</sub>*, *h<sub>42</sub>* phase plane (Fig. 5B). Upon an initial Ca<sup>2+</sup> release from one or more IP<sub>3</sub>R, a large spike is generated by Ca<sup>2+</sup>-induced Ca<sup>2+</sup> release (via the IP<sub>3</sub>R) during which time a decreasing *h<sub>42</sub>* gradually decreases the average open probability of the clustered IP<sub>3</sub>R. The spike is terminated when *h<sub>42</sub>* is too small to allow further Ca<sup>2+</sup> release. This phenomenon is qualitatively reproduced by the deterministic model (Fig. 5D). In both the stochastic and deterministic models the decrease in average IP<sub>3</sub>R open probability of a cluster of IP<sub>3</sub>R caused by Ca<sup>2+</sup> inhibition is the main reason for the termination of each spike.

According to Figs. 5B and D, regeneration of each spike requires a return of *h<sub>42</sub>* back to a relatively high value (i.e., recovery of the IP<sub>3</sub>R from inhibition by Ca<sup>2+</sup>). The deterministic model sets a clear threshold for the regeneration, as can be seen in Fig. 5C, where an upstroke in *c<sub>b</sub>* occurs when the trajectory creeps beyond the sharp “knee” of the white curve. When the trajectory reaches the knees of the white curve it is forced to jump across to the other stable branch of the critical manifold, resulting in a fast increase in *c<sub>b</sub>* followed by a relatively fast increase in *c* (seen by combining Figs. 5C and D).

In contrast, the stochastic model enlarges the contributions of individual IP<sub>3</sub>R so that the generation of each spike is also effectively driven by random Ca<sup>2+</sup> release through the IP<sub>3</sub>R, which can be seen in the inset of Fig. 5B where the site of spike initiation (blue bar) exhibits significantly greater variation than that of spike termination (green bar). In spite of this, the essential similarities in phase plane behavior result in both deterministic and stochastic models making the same qualitative predictions in response to perturbations, such as changes in IP<sub>3</sub> concentration ([IP<sub>3</sub>]), Ca<sup>2+</sup> influx or efflux. In the following, we illustrate this by investigating a number of experimentally testable predictions. Due to the extensive importance of frequency encoding in many Ca<sup>2+</sup>-dependent processes, we focus particularly on the change of oscillation frequency in response to parameter perturbations. As a

side issue we also investigate how the oscillation baseline depends on physiologically important parameters.

### Dependence of oscillation frequency on IP<sub>3</sub> concentration

In many cell types a moderate increase in [IP<sub>3</sub>] increases the Ca<sup>2+</sup> oscillation frequency (see Fig. 2A in [11], Fig. 4E in [16] and Fig. 6B in [17]), a result that is reproduced by both model types (Fig. 6A). As [IP<sub>3</sub>] increases, the stochastic model increases the probability of the initial Ca<sup>2+</sup> release through the first open IP<sub>3</sub>R and of the following Ca<sup>2+</sup> release, thus shortening the average ISI. Although the oscillatory region of the deterministic model is strictly confined by bifurcations which do not apply to the stochastic model, the deterministic model can successfully replicate an increasing frequency by lowering the “knee” of the red curve in Fig. 5D and shortening the time spent from the termination point *c* to the initiation point *a* (thus shortening the ISI). Hence, although the deterministic model cannot be used to predict the exact values of [IP<sub>3</sub>] at which the oscillations begin and end, as stochastic effects predominate in these regions, it can be used to predict the correct qualitative trend in oscillation frequency.

### Dependence of oscillation frequency on Ca<sup>2+</sup> influx and efflux

In many cell types, including ASMC, transmembrane fluxes modulate the total intracellular Ca<sup>2+</sup> load (*c<sub>t</sub>*) on a slow time scale [16,18], and thereby modulate the oscillation frequency [19]. Experimental data can be seen in Fig. 8 in [16] and Fig. 2 in [18]. Figs. 6B and C show that both stochastic and deterministic models predict the same qualitative changes in oscillation frequency in response to changes in membrane fluxes (through membrane ATPase pumps and/or Ca<sup>2+</sup> influx channels such as receptor-operated channels or store-operated channels).

### Dependence of oscillation frequency on SERCA expression

The level of sarco/endoplasmic reticulum calcium ATPase (SERCA) expression (or capacity) is important for airway remodeling in asthma [20] and ASMC Ca<sup>2+</sup> oscillations [21]. We thus investigated the predictions of the two models in response to changes in SERCA expression (*V<sub>s</sub>*). As *V<sub>s</sub>* decreases, the deterministic model exhibits a decreasing frequency, in agreement with experimental data (see Figs. 3 and 4 in [21]). The same trend is seen in the stochastic model with only 20 IP<sub>3</sub>R (see Fig. 6D).

### Dependence of oscillation frequency on Ca<sup>2+</sup> buffer concentration

Calcium buffers have been shown to be able to change the ISI and spike duration, which in turn change the oscillation frequency [15,22]. We compared the effects on the two models of varying total buffer concentration (*B<sub>t</sub>*) by adding one buffer with relatively fast kinetics to the models (see *Materials and Methods* for details). In both models the frequency decreases as *B<sub>t</sub>* increases (see Fig. 6E), which is consistent with experimental data (Fig. 2B in [18]). This is not surprising, because increasing *B<sub>t</sub>* can decrease the effective rates of SR Ca<sup>2+</sup> release and reuptake.

### Dependence of oscillation baseline on Ca<sup>2+</sup> influx and SERCA expression

Sustained elevations of baseline during agonist-induced Ca<sup>2+</sup> oscillations or transients have been observed experimentally, and are believed to be a result of an increase in Ca<sup>2+</sup> influx caused by opening of membrane Ca<sup>2+</sup> channels [13,16]. Furthermore, there

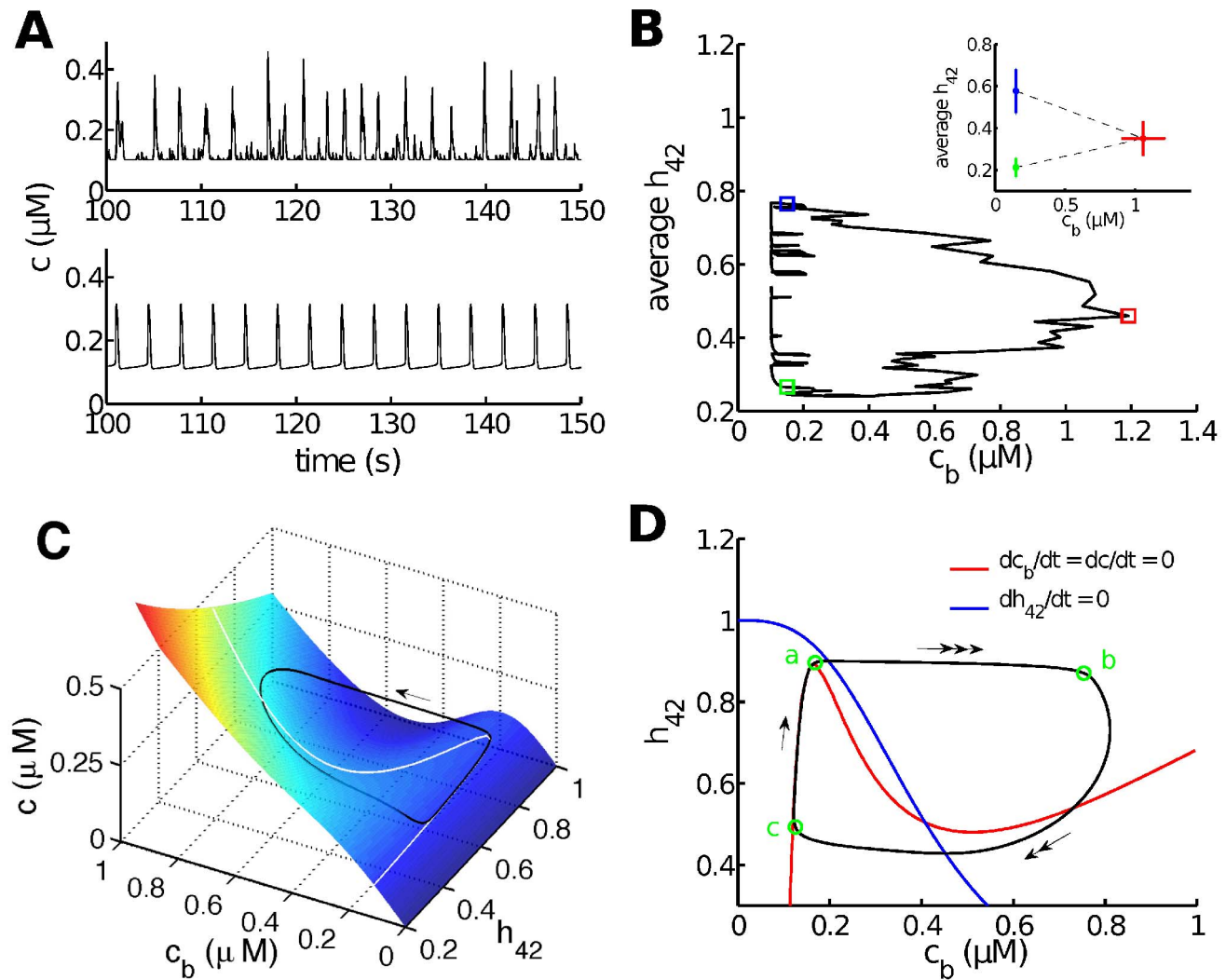


**Figure 5. Stochastic and deterministic simulations exhibit similar dynamic properties.** **A:** simulated stochastic (upper panel) or deterministic (lower panel)  $\text{Ca}^{2+}$  oscillations at  $0.1 \mu\text{M}$   $\text{IP}_3$ . **B:** a typical stochastic solution projected on the  $c_b-h_{42}$  plane. The average  $h_{42}$  represents the average value of  $h_{42}$  over the 20  $\text{IP}_3\text{R}$ . Statistics (mean  $\pm$  SD) of the initiation point (blue square), the peak (red square) and termination point (green square) are shown in the inset. 116 samples are obtained by applying a low threshold of  $0.15 \mu\text{M}$  and a high threshold of  $0.8 \mu\text{M}$  to  $c_b$ . **C:** a typical periodic solution of the deterministic model (black curve), plotted in the  $c, c_b, h_{42}$  phase space. The arrow indicates the direction of movement.  $c_t$  is the slowest variable so that its variation during an oscillation is very small. This allows to treat  $c_t$  as a constant ( $c_t = 53.12 \mu\text{M}$  in this case) and study the dynamics of the model in the  $c, c_b, h_{42}$  phase space. The color surface is the surface where  $dc_b/dt=0$  (called the critical manifold). The white N-shaped curve is the intersection of the critical manifold and the surface  $dc/dt=0$ . **D:** projection of the periodic solution to the  $c_b, h_{42}$  plane. The red N-shaped curve is the projection to the  $c_b, h_{42}$  plane of the white curve shown in **C**. The evolution of the deterministic solution exhibits three different time scales separated by green circles (labelled by a, b and c) and indicated by arrows (triple arrow: fastest; double arrow: intermediate; single arrow: slowest).  
doi:10.1371/journal.pcbi.1003783.g005

is evidence showing that decreased SERCA expression could also increase the baseline (Fig. 4 in [21]). Those phenomena are successfully reproduced by both models (see Fig. 7).

## Discussion

In this paper we address two current major questions in the field of  $\text{Ca}^{2+}$  modeling. Firstly, we show that  $\text{Ca}^{2+}$  puffs and stochastic oscillations can be reproduced quantitatively by an extremely simple model, consisting only of two states (one open, one closed), with time-dependent transitions between them. This model is obtained by removing the intramodal structure of a more complex model that was determined by fitting a Markov model to single-

channel data [7]. We thus show that the internal structure of each mode is irrelevant for function and mode switching is the key mechanism for the control of calcium release. The necessity for time-dependent mode switching is shown not only by the dynamic single-channel data of [4]), but also by the puff data of [9] and our ASMC data.

Secondly, we investigate the role of stochasticity of  $\text{IP}_3\text{R}$  in modeling  $\text{Ca}^{2+}$  oscillations in ASMC by comparing a stochastic  $\text{IP}_3\text{R}$ -based  $\text{Ca}^{2+}$  model and its associated deterministic version, for parameters such that both of the models exhibit  $\text{Ca}^{2+}$  spikes but the stochastic model cannot necessarily be replaced by a mean-field model. We find that a four-variable deterministic model has the same predictive power as the stochastic model, in

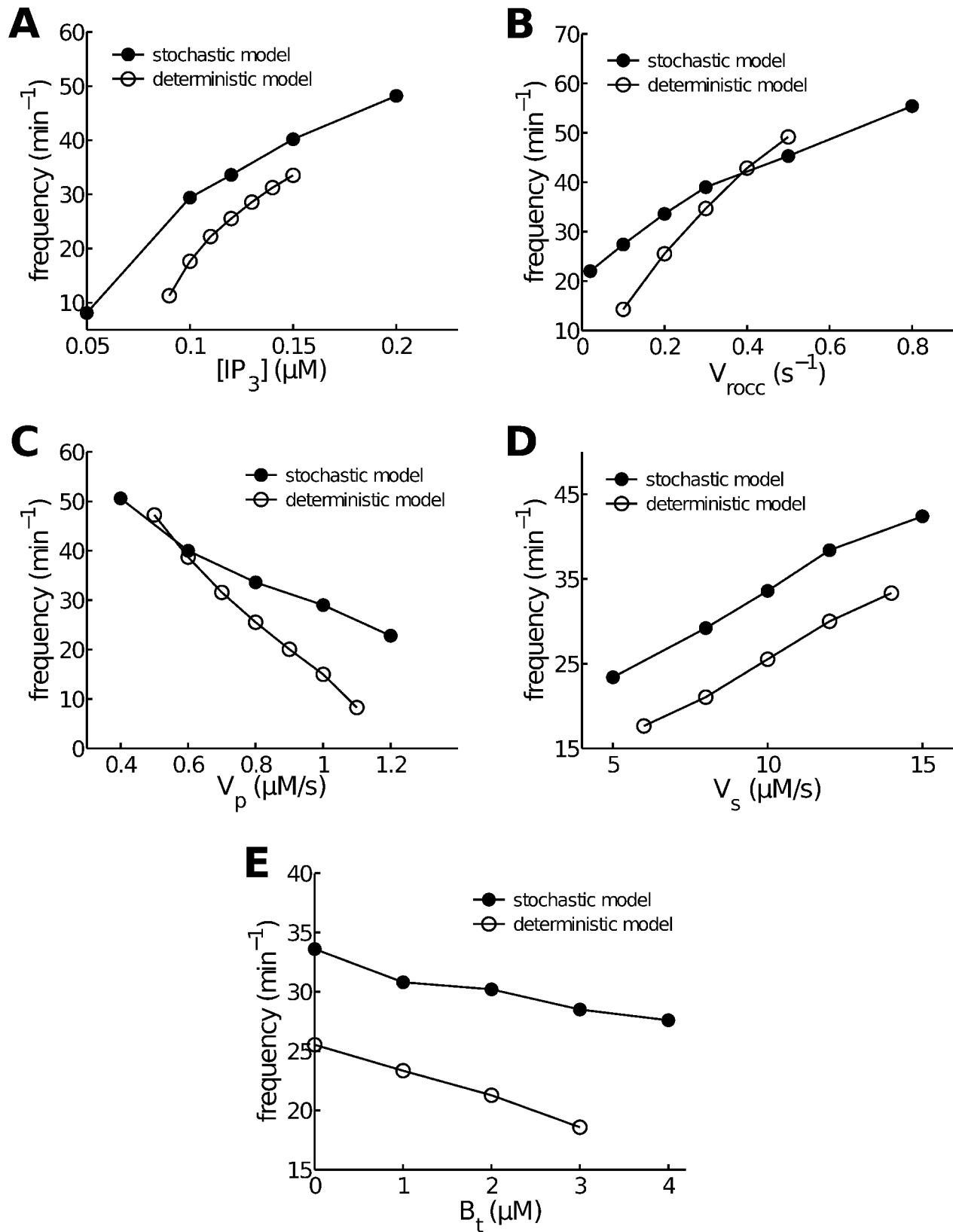


**Figure 6. Comparison of parameter-dependent frequency changes in the stochastic and deterministic models.** All curves are computed at 0.12 μM IP<sub>3</sub> except in panel A, which uses a variety of [IP<sub>3</sub>]. Other parameters are set at their default values given in Table 1. **A:** as [IP<sub>3</sub>] increases, Ca<sup>2+</sup> oscillations in both models increase in frequency. **B:** as Ca<sup>2+</sup> influx increases (modeled by an increase in receptor-operated calcium channel flux coefficient V<sub>rocc</sub>), so does the oscillation frequency in both models. **C:** as Ca<sup>2+</sup> efflux increases (modeled by an increase in plasma pump expression V<sub>p</sub>), oscillation frequency decreases. **D:** as SERCA pump expression, V<sub>s</sub>, increases, so does oscillation frequency. **E:** as total buffer concentration, B<sub>t</sub>, increases, oscillation frequency decreases.  
doi:10.1371/journal.pcbi.1003783.g006



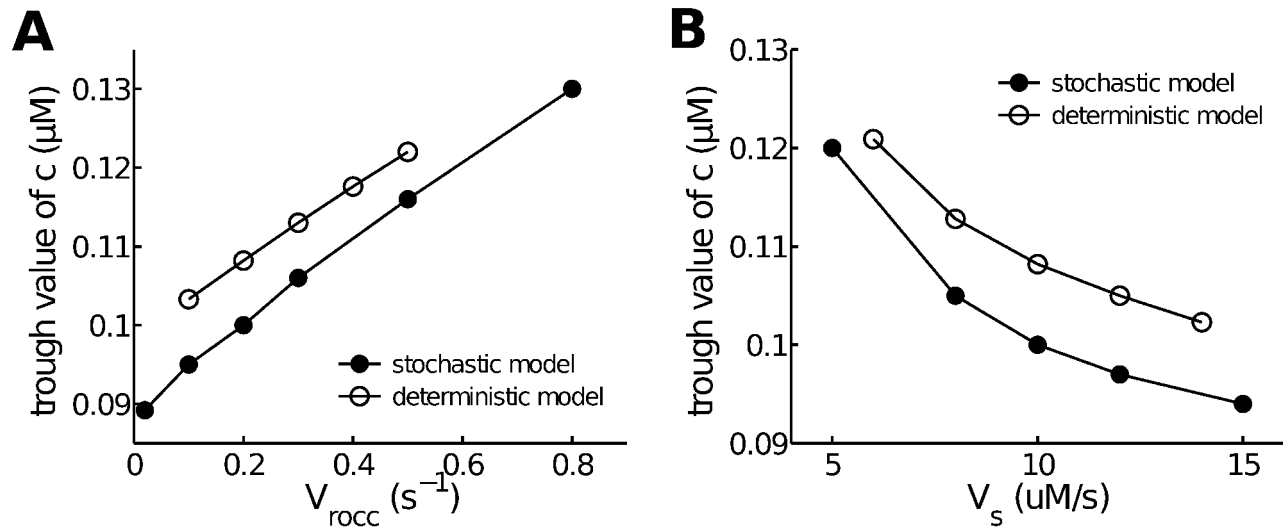


**Figure 7. Dependence of calcium oscillation baseline on calcium influx and SERCA expression.** **A:** increasing influx (described by  $V_{rocc}$ ) increases the average trough of  $Ca^{2+}$  oscillations. **B:** decreasing SERCA expression (described by  $V_s$ ) increases the average trough of  $Ca^{2+}$  oscillations. All curves are computed at  $0.12 \mu M$   $IP_3$ . doi:10.1371/journal.pcbi.1003783.g007

that it correctly reproduces the process of spike termination and predicts the same qualitative changes in oscillation frequency and baseline in response to a variety of perturbations that are commonly used experimentally. The mechanism for termination of individual spikes is fundamentally a deterministic process controlled by a rapid inhibition induced by the high local  $[Ca^{2+}]_i$  in the  $IP_3R$  cluster, whereas spike initiation is significantly affected by stochastic opening of  $IP_3R$ . Hence, repetitive  $Ca^{2+}$  cycling is primarily induced by the time-dependent gating variables governing transitions of the  $IP_3R$  from one mode to another.

Our simplified two-state model of the  $IP_3R$  is identical in structure (although not in parameter values) to the well-known model of [23]. It is somewhat ironic that after 20 years of detailed studies of the  $IP_3R$  and the construction of a plethora of models of varying complexity, the single-channel data have led us around full circle, back to these original formulations. Excitability is arising via a fast activation

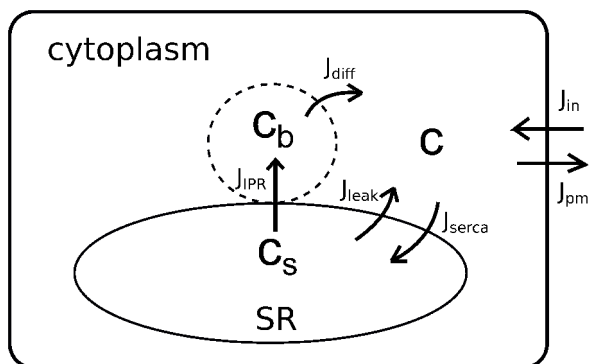


**Figure 8. Schematic diagram of the  $Ca^{2+}$  model.**  $c$  represents cytoplasmic  $Ca^{2+}$  concentration, excluding a small local  $Ca^{2+}$  (whose concentration is denoted by  $c_b$ ) close to the  $Ca^{2+}$  release site (i.e., an  $IP_3R$  cluster). Upon coordinated openings of the  $IP_3R$ , SR  $Ca^{2+}$  ( $c_s$ ) is first released into the local domain ( $J_{IPR}$ ) to cause a rapid increase in  $c_b$ . High local  $Ca^{2+}$  then diffuses to the rest of the cytoplasm ( $J_{diff}$ ), and is eventually pumped back to the SR ( $J_{serca}$ ). doi:10.1371/journal.pcbi.1003783.g008

followed by a slower inactivation, a combination often seen in physiological processes [24]. Encoding of this fundamental combination results directly from the two-mode structure of the  $IP_3R$ . Although similar single-channel data have been used to construct three-mode models [6,25], neither of these models has yet been used in detailed studies of  $Ca^{2+}$  puffs and waves, and it remains unclear whether or not they have a similar underlying structure.

In contrast to previous deterministic ODE models, our four-variable  $Ca^{2+}$  model includes a more accurate  $IP_3R$  model, as well as local control of clustered  $IP_3R$  by two distinct  $Ca^{2+}$  microdomains; one at the mouth of an open  $IP_3R$ , the other inside a cluster of  $IP_3R$ . Neglect of either of these microdomains leads to models that either exhibit unphysiological cytoplasmic  $Ca^{2+}$  concentrations or fail to reproduce reasonable oscillations. This underlines the importance of taking  $Ca^{2+}$  microdomains into consideration when constructing any model. Our microdomain model is highly simplified, with the microdomain being treated simply as a well-mixed compartment. More detailed modeling of spatially-dependent microdomains is possible, and not difficult in principle, but requires far greater computational resources. It is undeniable that a more detailed model, incorporating the full spatial complexity – and possibly stochastic aspects as well – would make, overall, a better predictive tool. However, our goal is to find the simplest models that can be used as predictive tools.

An important similar study is that of Shuai and Jung [26]. They compared the use of Markov and Langevin approaches to the computation of puff amplitude distributions, compared their results with the deterministic limit, and showed that  $IP_3R$  stochasticity does not qualitatively change the type of puff amplitude distribution except for when there are fewer than 10  $IP_3R$ . Here, we significantly extend the scope of their study by exploring the effects of  $IP_3R$  stochasticity on the dynamics of  $Ca^{2+}$  spikes, and we do this in the context of an  $IP_3R$  model that has been fitted to single-channel data. Although this is true in a general sense for the Li-Rinzel model, which is based on the DeYoung-Keizer model, which did take into account the opening time distributions of  $IP_3R$  in lipid bilayers, neither model can reproduce the more recent data obtained from on-nuclei patch clamping. When these recent data are taken into account one obtains a model with the same structure, but quite different parameters and behavior.

**Table 1.** Parameter values of the stochastic calcium model.

Parameter	Description	Value/Units
$k_{\text{IP}_3\text{R}}$	IP <sub>3</sub> R flux coefficient	0.05 s <sup>-1</sup>
$k_{\text{diff}}$	Ca <sup>2+</sup> diffusional flux coefficient	10 s <sup>-1</sup>
$k_{\text{leak}}$	SR leak flux coefficient	0.0032 s <sup>-1</sup>
$V_s$	maximum capacity of SERCA	10 μM·s <sup>-1</sup>
$K_s$	SERCA half-maximal activating [Ca <sup>2+</sup> ] <sub>i</sub>	0.26 μM
$n_s$	Hill coefficient for SERCA	1.75
$J_{\text{leakin}}$	plasma membrane leak influx	0.03115 μM·s <sup>-1</sup>
$V_{\text{rocc}}$	ROCC flux coefficient	0.2 s <sup>-1</sup>
$V_{\text{socc}}$	maximum capacity of SOCC	1.6 μM·s <sup>-1</sup>
$K_{\text{socc}}$	SOCC dissociation constant	100 μM
$V_p$	maximum capacity of plasma pump	0.8 μM·s <sup>-1</sup>
$K_p$	half-maximal activating [Ca <sup>2+</sup> ] <sub>i</sub> of plasma pump	0.5 μM
$n_p$	Hill coefficient for plasma pump	2
$\gamma_1$	the cytoplasmic-to-microdomain volume ratio	100
$\gamma_2$	the cytoplasmic-to-SR volume ratio	10
$c_{p0}$	an instantaneous high [Ca <sup>2+</sup> ] <sub>i</sub> at open channel pore when $c_s = 100$ μM	120 μM
$N_I$	total number of IP <sub>3</sub> R channels	20

doi:10.1371/journal.pcbi.1003783.t001

We find that, in spite of a relatively large variation in spike amplitude which is partially caused by a large variation in ISI (Fig. 5B), the mechanism governing individual spike terminations is the same for both a few or infinitely many IP<sub>3</sub>R, which explains why the one-peak type of amplitude distribution is independent of the choice of IP<sub>3</sub>R number (see Fig. 6A in [26]).

Another important relevant study was done by Dupont et al. [27], who compared the regularity of stochastic oscillations in hepatocytes for different numbers of IP<sub>3</sub>R clusters. They found that the impact of IP<sub>3</sub>R stochasticity on global Ca<sup>2+</sup> oscillations (in terms of CV) increases as the total cluster number decreases. Our study here extends these results, and demonstrates how well stochastic oscillations can be qualitatively described by a deterministic system, even when there is only a small number of IP<sub>3</sub>R (which appears to be the case for ASMC, in which the wave initiation site is only 2~4 μm in diameter). Indeed, as we have shown, for the purposes of predictive modeling a simple deterministic model does as well as more complex stochastic simulations.

Ryanodine receptors (RyR) are another important component modulating ASMC Ca<sup>2+</sup> oscillations [16,28,29] but are not included in our model. This is because the role of RyR is not fully understood and may be species-dependent; for example, in mouse or human ASMC, RyR play very little role in IP<sub>3</sub>-induced continuing Ca<sup>2+</sup> oscillations [17,30], but this appears not to be true for pigs [28]. Our study focuses on the calcium oscillations in mouse and human (as we did in our experiments) where inclusion of a deterministic model of RyR should have little effect. An understanding of the role of RyR stochasticity and how the IP<sub>3</sub>R and the RyR interact needs a reliable RyR Markov model, exclusive to ASMC, which is not currently available. Multiple Markov models of the RyR have been developed for use in cardiac cells [31], but these are based on single-channel data from lipid bilayers, and are adapted for the specific context of cardiac cells. Their applicability to ASMC remains unclear.

Although we have not shown that the deterministic model for ASMC has the same predictive power as the stochastic model in all possible cases (which would hardly be possible in the absence of an analytical proof) the underlying similarity in phase plane structure indicates that such similarity is plausible at least. Certainly, we have not found any counterexample to this claim. However, whether or not this claim is true for all cell types is unclear. Some cell types exhibit both local Ca<sup>2+</sup> puffs and global Ca<sup>2+</sup> spikes (usually propagating throughout the cells in the form of traveling waves), showing that initiation of such Ca<sup>2+</sup> spikes requires a synchronization of Ca<sup>2+</sup> release from more than one cluster of IP<sub>3</sub>R [14]. This type of spiking relies on the hierarchical organization of Ca<sup>2+</sup> signal pathways, in particular the stochastic recruitment of both individual IP<sub>3</sub>R and puffs at different levels [32], and therefore cannot be simply reproduced by deterministic models containing only a few ODEs. However, Ca<sup>2+</sup> oscillations in ASMC, as observed in lung slices, may not be of this type, as IP<sub>3</sub>R-dependent puffs have not been seen in these ASMC. It thus appears that, in ASMC in lung slices, every Ca<sup>2+</sup> ‘‘puff’’ initiates a wave, resulting in periodic waves with ISI that are governed by the dynamics of individual puffs.

## Materials and Methods

### Ethics Statement

Animal experimentations carried out were approved by the Animal Care and Use Committee of the University of Massachusetts Medical School under approval number A-836-12.

### Lung slice preparation

BALB/c mice (7–10 weeks old, Charles River Breeding Labs, Needham, MA) were euthanized via intraperitoneal injection of 0.3 ml sodium pentobarbitone (Oak Pharmaceuticals, Lake Forest,

IL). After removal of the chest wall, lungs were inflated with  $\sim 1.1$  ml of 1.8% warm agarose in sHBSS via an intratracheal catheter. Subsequently, air ( $\sim 0.3$  ml) was injected to push the agarose within the airways into the alveoli. The agarose was polymerized by cooling to  $4^\circ\text{C}$ . A vibratome (VF-300, Precisionary Instruments, San Jose, CA) was used to make  $180\ \mu\text{m}$  thick slices which were maintained in Dulbecco's Modified Eagle's Media (DMEM, Invitrogen, Carlsbad, CA) at  $37^\circ\text{C}$  in 10%  $\text{CO}_2/\text{air}$ . All experiments were conducted at  $37^\circ\text{C}$  in a custom-made temperature-controlled Plexiglas chamber as described in [17].

### Measurement of $\text{Ca}^{2+}$ oscillations

Lung slices were incubated in sHBSS containing  $20\ \mu\text{M}$  Oregon Green 488 BAPTA-1-AM (Invitrogen), a  $\text{Ca}^{2+}$ -indicator dye, 0.1% Pluronic F-127 (Invitrogen) and  $200\ \mu\text{M}$  sulfobromophthalein (Sigma Aldrich, St Louis, MO) in the dark at  $30^\circ\text{C}$  for 1 hour. Subsequently, the slices were incubated in  $200\ \mu\text{M}$  sulfobromophthalein for 30 minutes. Slices were mounted on a cover-glass and held down with  $200\ \mu\text{m}$  mesh. A smaller cover-glass was placed on top of the mesh and sealed at the sides with silicone grease to facilitate solution exchange. Slices were examined with a custom-built 2-photon scanning laser microscope with a  $\times 40$  oil immersion objective lens and images recorded at 30 images per second using Videosavant 4.0 software (IO Industries, Montreal, Canada). Changes in fluorescence intensity (which represent changes in  $[\text{Ca}^{2+}]_i$ ) were analyzed in an ASMC of interest by averaging the grey value of a  $10 \times 10$  pixel region using custom written software. Relative fluorescence intensity ( $F/F_0$ ) was expressed as a ratio of the fluorescence intensity at a particular time ( $F$ ) normalized to the initial fluorescence intensity ( $F_0$ ).

### The calcium model

Inhomogeneity of cytoplasmic  $\text{Ca}^{2+}$  concentration not only exists around individual channel pores of the  $\text{IP}_3\text{R}$ , where a nearly instantaneous high  $\text{Ca}^{2+}$  concentration at the pore (denoted by  $c_p$ ) leads to a very sharp concentration profile, but is also seen inside an  $\text{IP}_3\text{R}$  cluster where the average cluster  $\text{Ca}^{2+}$  concentration ( $c_b$ ) is apparently higher than that of the surrounding cytoplasm ( $c$ ) [33]. This indicates that during  $\text{Ca}^{2+}$  oscillations each  $\text{IP}_3\text{R}$  is controlled by either the pore  $\text{Ca}^{2+}$  concentration (when it is open) or the cluster  $\text{Ca}^{2+}$  concentration (when it is closed). Neither of these local concentrations influence cell membrane fluxes or the majority of SERCAs, which we assume to be distributed outside the cluster.

The scale separation between the pore  $\text{Ca}^{2+}$  concentration and the cluster  $\text{Ca}^{2+}$  concentration allows to treat  $c_p$  as a parameter, providing a simpler way of modeling local  $\text{Ca}^{2+}$  events (like  $\text{Ca}^{2+}$  puffs) that has been used in several previous studies [8,34,35]. However, evolution of the cluster concentration and wide-field cytoplasm  $\text{Ca}^{2+}$  concentration are not always separable, so an additional differential equation for the cluster  $\text{Ca}^{2+}$  is necessary.

A schematic diagram of the model is shown in Fig. 8. The corresponding ODEs are

$$\frac{dc}{dt} = J_{\text{diff}} + J_{\text{leak}} - J_{\text{serca}} + J_{\text{in}} - J_{\text{pm}}, \quad (1)$$

$$\frac{dc_b}{dt} = \gamma_1(J_{\text{IPR}} - J_{\text{diff}}), \quad (2)$$

$$\frac{dc_t}{dt} = J_{\text{in}} - J_{\text{pm}}, \quad (3)$$

where  $c_t = c + c_b/\gamma_1 + c_s/\gamma_2$  representing total intracellular  $\text{Ca}^{2+}$  concentration, and thus SR  $\text{Ca}^{2+}$  concentration,  $c_s$  is given by  $c_s = \gamma_2(c_t - c - c_b/\gamma_1)$ .  $\gamma_1$  and  $\gamma_2$  are the volume ratios given in Table 1.  $J_{\text{IPR}}$  is the flux through the  $\text{IP}_3\text{R}$ ,  $J_{\text{leak}}$  is a background  $\text{Ca}^{2+}$  leak out of the SR, and  $J_{\text{serca}}$  is the uptake of  $\text{Ca}^{2+}$  into the SR by SERCA pumps.  $J_{\text{pm}}$  is the flux through plasma pump, and  $J_{\text{in}}$  represents a sum of main  $\text{Ca}^{2+}$  influxes including  $J_{\text{rocc}}$  (receptor-operated  $\text{Ca}^{2+}$  channel),  $J_{\text{socc}}$  (store-operated  $\text{Ca}^{2+}$  channel) and  $J_{\text{leakin}}$  ( $\text{Ca}^{2+}$  leak into the cell).  $J_{\text{diff}}$  coarsely models the diffusion flux from cluster microdomain to the cytoplasm. Details of the fluxes are

- Different formulations of  $J_{\text{IPR}}$  give different types of models:

- For the stochastic model,  $J_{\text{IPR}} = (k_{\text{IPR}}/N_t)N_o(c_s - c)$  where  $k_{\text{IPR}}$  is the maximum conductance of a cluster of  $N_t$   $\text{IP}_3\text{R}$  (here  $N_t = 20$ ).  $N_o$  is the number of open  $\text{IP}_3\text{R}$  determined by the states of  $\text{IP}_3\text{R}$ .
- For the deterministic model we set  $J_{\text{IPR}} = k_{\text{IPR}}P_o(c_s - c)$  where  $P_o$  is the  $\text{IP}_3\text{R}$  open probability, a continuous analogue of  $N_o/N_t$ .

To calculate  $N_o$  and  $P_o$ , we use the  $\text{IP}_3\text{R}$  model of [7,8], with minor modifications described later.

- $J_{\text{diff}} = k_{\text{diff}}(c_b - c)$ .

- $J_{\text{serca}} = V_s c^{n_s} / (K_s^{n_s} + c^{n_s})$  where  $K_s$  and  $n_s$  are obtained from [36].

- $J_{\text{leak}} = k_{\text{leak}}(c_s - c)$ .

- $J_{\text{in}}$  includes a basal leak ( $J_{\text{leakin}}$ ), receptor-operated calcium channel (ROCC,  $J_{\text{rocc}}$ ), store-operated calcium channel (SOCC,  $J_{\text{socc}}$ ). By using the  $\text{IP}_3$  concentration ( $p$ ) as a surrogate indicator of MCh concentration, we assume that  $J_{\text{rocc}} = V_{\text{rocc}}p$ .  $\text{S O C C i s m o d e l e d b y } J_{\text{socc}} = V_{\text{socc}}K_{\text{socc}}^4 / (K_{\text{socc}}^4 + c_s^4)$  [13].

- $J_{\text{pm}} = V_p c^{n_p} / (K_p^{n_p} + c^{n_p})$ .

Calcium concentration at open channel pore ( $c_p$ ) does not explicitly appear in the equations but is used in the  $\text{IP}_3\text{R}$  model introduced later.  $c_p$  is assumed to be proportional to SR  $\text{Ca}^{2+}$  concentration ( $c_s$ ) and is therefore simply modeled by

**Table 2.** Parameter values of the IP<sub>3</sub>R model.

Parameter	Value/Units	Parameter	Value/Units
$q_{12}$	1240 s <sup>-1</sup>	$q_{21}$	88 s <sup>-1</sup>
$q_{23}$	3 s <sup>-1</sup>	$q_{32}$	69 s <sup>-1</sup>
$q_{26}$	10500 s <sup>-1</sup>	$q_{62}$	4010 s <sup>-1</sup>
$q_{45}$	11 s <sup>-1</sup>	$q_{54}$	3330 s <sup>-1</sup>
$H$	20 s <sup>-1</sup>	$L$	0.5 s <sup>-1</sup>
$\lambda_{m_{24}}$	100 s <sup>-1</sup>	$\lambda_{m_{42}}$	100 s <sup>-1</sup>
$\lambda_{h_{24}}$	40 s <sup>-1</sup>		

doi:10.1371/journal.pcbi.1003783.t002

$c_p = c_{p0}(c_s/100)$  where  $c_{p0}$  is the value corresponding to  $c_s = 100 \mu\text{M}$ . Alternatively,  $c_p$  can also be assumed to be a large constant (say greater than  $100 \mu\text{M}$ ) without fundamentally altering the model dynamics. The choice of  $c_{p0}$  is not critical as long as it is sufficiently large to play a role in inactivating the open channels. All the parameter values are given in Table 1.

### The data-driven IP<sub>3</sub>R model

The IP<sub>3</sub>R model used in our ASMC calcium model is an improved version of the Siekmann IP<sub>3</sub>R model which is a 6-state Markov model derived by fitting to the stationary single channel data using Markov chain Monte Carlo (MCMC) [5,7,8]. Fig. 1 has shown the structure of the IP<sub>3</sub>R model which is comprised of two modes; the drive mode, containing three closed states  $C_1, C_2, C_3$  and one open state  $O_6$ , and the park mode, containing one closed state  $C_4$  and one open state  $O_5$ . The transition rates in each mode are constants (shown in Table 2), but  $q_{42}$  and  $q_{24}$  which connect the two modes are Ca<sup>2+</sup>-/IP<sub>3</sub>-dependent and are formulated as

$$q_{24} = a_{24} + V_{24}(1 - m_{24}h_{24}), \quad (4)$$

$$q_{42} = a_{42} + V_{42}m_{42}h_{42}, \quad (5)$$

where  $m_{24}, h_{24}, m_{42}$  and  $h_{42}$  are Ca<sup>2+</sup>-/IP<sub>3</sub>-modulated gating variables.  $a_{24}, a_{42}, V_{24}$  and  $V_{42}$  are either functions of  $p$  or constants and are given later. We assume the gating variables obey the following differential equation,

$$\frac{dG}{dt} = \lambda_G(G_\infty - G), \quad (G = m_{24}, h_{24}, m_{42}, h_{42}), \quad (6)$$

where  $G_\infty$  is the equilibrium and  $\lambda_G$  is the rate at which the equilibrium is approached. Those equilibria are functions of Ca<sup>2+</sup> concentration at the cytoplasmic side of the IP<sub>3</sub>R, denoted by  $\hat{c}$  in the equations, equal to either  $c_p$  or  $c_b$  depending on the state of the channel). They are assumed to be

$$m_{24\infty} = \frac{\hat{c}^3}{\hat{c}^3 + k_{24}^3}, \quad (7)$$

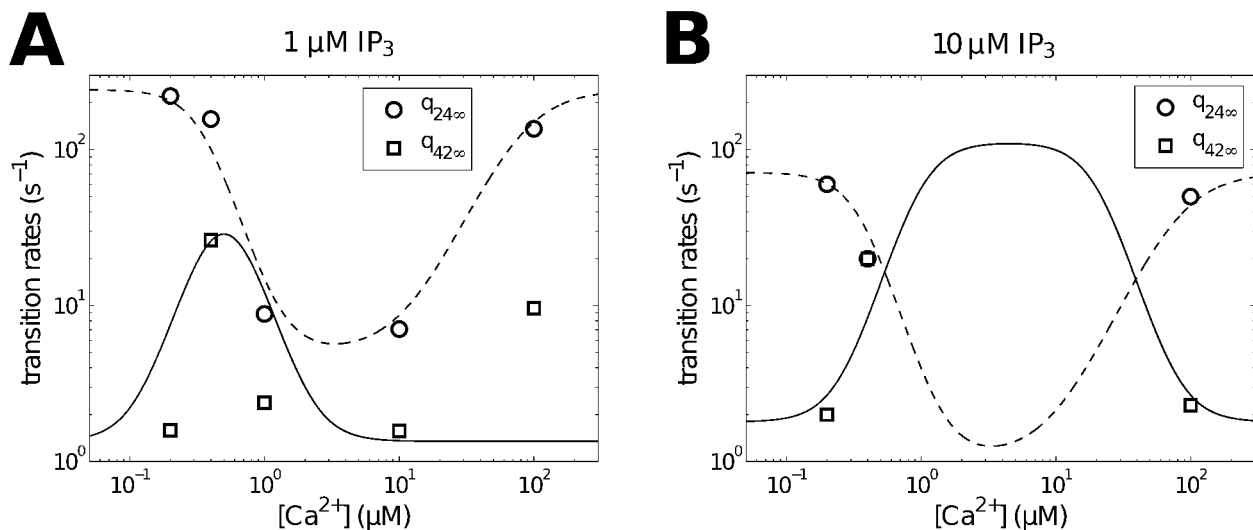


**Figure 9. Stationary data and fits of  $q_{24}$  and  $q_{42}$ .** Stationary transition rates of  $q_{24}$  and  $q_{42}$ ,  $q_{24\infty}$  and  $q_{42\infty}$ , as functions of Ca<sup>2+</sup> concentration were estimated and fitted for two [IP<sub>3</sub>], 1 μM (A) and 10 μM (B). Circles and squares represent the means of  $q_{24}$  and  $q_{42}$  distributions computed by MCMC simulation [7]. Note that MCMC failed to determine the values of  $q_{24}$  and  $q_{42}$  at  $\hat{c} = 1, 10 \mu\text{M}$  for 10 μM IP<sub>3</sub>, as the IP<sub>3</sub>R was almost in the drive mode for these cases. The corresponding fitting curves (solid for  $q_{42}$ ; dashed for  $q_{24}$ ) are produced using Eqs. 7–12. doi:10.1371/journal.pcbi.1003783.g009

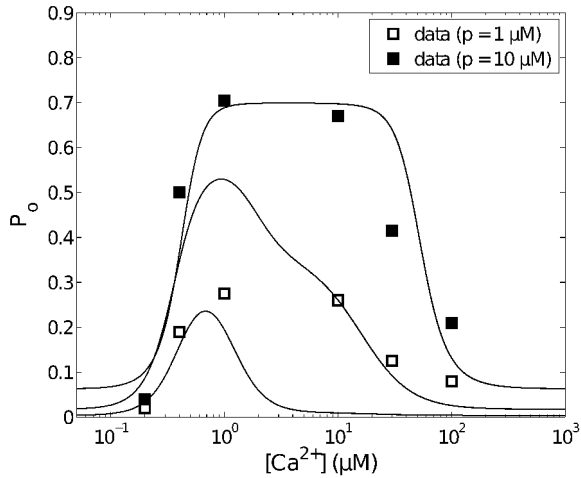


**Figure 10. Open probability curves for various  $[IP_3]$ .**  $P_o$  is equal to the sum of probabilities of the  $IP_3R$  in  $O_5$  and  $O_6$ . Three representative curves correspond to  $0.1 \mu M$ ,  $1 \mu M$  and  $10 \mu M$   $[IP_3]$  (from bottom to top) respectively. Data (average open probability) are from [5].

doi:10.1371/journal.pcbi.1003783.g010

$$h_{24\infty} = \frac{k_{-24}^2}{\hat{c}^2 + k_{-24}^2}, \quad (8)$$

$$m_{42\infty} = \frac{\hat{c}^3}{\hat{c}^3 + k_{42}^3}, \quad (9)$$

$$h_{42\infty} = \frac{k_{-42}^3}{\hat{c}^3 + k_{-42}^3}. \quad (10)$$

Hence, we have stationary expressions of  $q_{42}$  and  $q_{24}$ ,

$$q_{24\infty} = a_{24} + V_{24}(1 - m_{24\infty}h_{24\infty}), \quad (11)$$

$$q_{42\infty} = a_{42} + V_{42}m_{42\infty}h_{42\infty}. \quad (12)$$

The expressions of  $a_s$ ,  $V_s$ ,  $n_s$  and  $k_s$  are chosen as follows so that Eq. 11 and Eq. 12 capture the correct trends of experimental values of  $q_{24}$  and  $q_{42}$  (see Fig. 9) and generate relatively smooth open probability curves (see Fig. 10),

$$\begin{aligned} V_{24} &= 62 + 880/(p^2 + 4) & a_{24} &= 1 + 5/(p^2 + 0.25) \\ V_{42} &= 110p^2/(p^2 + 0.01) & a_{42} &= 1.8p^2/(p^2 + 0.34) \\ k_{24} &= 0.35 & k_{42} &= 0.49 + 0.543p^3/(p^3 + 64) \\ k_{-24} &= 80 & k_{-42} &= 0.41 + 25p^3/(p^3 + 274.6) \end{aligned}$$

Note that the above formulas are different from the relatively complicated formulas used in [8]. The rates,  $\lambda_{m_{24}}$ ,  $\lambda_{h_{24}}$  and  $\lambda_{m_{42}}$ , are constants estimated by using dynamic single channel data [4] and

given in Table 2, whereas  $\lambda_{h_{42}}$  is not clearly revealed by experimental data. However we have shown that it should be relatively large for high  $\hat{c}$  but relatively small for low  $\hat{c}$  for reproducing experimental puff data [8]. By introducing two  $Ca^{2+}$  concentrations,  $c_b$  and  $c_p$ ,  $\lambda_{h_{42}}$  and the state of the  $IP_3R$  channel become highly correlated, so that we can assume  $\lambda_{h_{42}}$  is a relatively large value  $H$  if the channel is open and is a relatively small value  $L$  if the channel is closed. Hence,  $\lambda_{h_{42}}$  is modeled by the logic function

$$\lambda_{h_{42}} = \begin{cases} H, & \text{if the channel is open;} \\ L, & \text{if the channel is closed.} \end{cases}$$

Values of  $L$  and  $H$  are chosen so that simulated  $Ca^{2+}$  oscillations in ASMC are comparable to experimental observations.

### The $IP_3R$ model reduction

Here we reduce the 6-state model to a 2-state open/closed model. The reduction takes the following steps:

- The sum of the probabilities of  $C_1$ ,  $C_3$  and  $O_5$  is less than 0.03 for any  $\hat{c}$ , so they are either rarely visited by the  $IP_3R$  or have a very short dwell time. This implies they have very little contribution to the  $Ca^{2+}$  dynamics. Therefore, we completely remove the three states from the full model.
- Transition rates of  $q_{26}$  and  $q_{62}$  are about 2 orders larger than that of  $q_{24}$  and  $q_{42}$ , which allows us to omit the fast transitions by taking a quasi-steady state approximation. This change will affect two aspects. First, we have  $O_6 = C_2q_{26}/q_{62}$  which allows us to combine  $C_2$  and  $O_6$  to be a new state  $D$ , which satisfies  $D = O_6(q_{62} + q_{26})/q_{26}$ . Although this means  $D$  is a partially open state with an open probability of  $q_{26}/(q_{62} + q_{26})$ , it can be used as an fully open state in the stochastic simulations by multiplying the maximum  $IP_3R$  flux conductance  $k_{IPR}$  by a factor of  $q_{26}/(q_{62} + q_{26})$ . Secondly,  $q_{24}$  needs to be rescaled by  $q_{62}/(q_{62} + q_{26})$ , i.e., the effective closing rate is  $q_{24}q_{62}/(q_{62} + q_{26})$ .
- Due to the combination of  $C_2$  and  $O_6$ ,  $\lambda_h$  is accordingly modified to

$$\lambda_{h_{42}} = \begin{cases} H, & \text{if the channel is in } C_4 \\ L, & \text{if the channel is in } D \text{ (the drive mode)} \end{cases}$$

Hence, the reduced two-state model contains one ‘‘open’’ state  $D$  and one closed state  $C_4$  with the opening transition rate of  $q_{42}$  and the closing transition rate of  $q_{24}q_{62}/(q_{62} + q_{26})$ .

### Deterministic formulation of the stochastic model

Based on the stochastic calcium model and the reduced 2-state  $IP_3R$  model, we construct a deterministic model. We need to modify three things that are used in the stochastic model but inapplicable to fast simulations of the deterministic model. The first is the discrete number of open channels; the second is state-dependent use of  $c_b$  and  $c_p$  in calculating  $q_{42}$  and  $q_{24}$ ; the last is the logic expression of  $\lambda_{h_{42}}$ . Details of the modifications are as follows,

- The fraction of open channels ( $N_o/N_t$ ) is replaced by open probability  $P_o$  which is 70% of the probability of state  $D$ .

- In the stochastic simulations,  $q_{24}$  which only controls the IP<sub>3</sub>R closing is primarily governed by  $c_p$ , whereas  $q_{42}$  which controls IP<sub>3</sub>R opening is mainly governed by  $c_b$ . Therefore, in the deterministic model, we separate the functions of  $c_p$  and  $c_b$  by assuming  $m_{24\infty}$  and  $h_{24\infty}$  are functions of  $c_p$  only whereas  $m_{42\infty}$  and  $h_{42\infty}$  are functions of  $c_b$  only. That is,  $m_{24\infty} = m_{24\infty}(c_p)$ ,  $h_{24\infty} = h_{24\infty}(c_p)$ ,  $m_{42\infty} = m_{42\infty}(c_b)$  and  $h_{42\infty} = h_{42\infty}(c_b)$ . Here  $c_p = c_{p0}(c_s/100)$  as defined before.
- To describe an average rate that infinitely many receptors are rapidly inhibited by high Ca<sup>2+</sup> concentration but slowly restored from Ca<sup>2+</sup>-inhibition.  $\lambda_{h_{42}}$  is proposed to be

$$\lambda_{h_{42}} = (1-D)L + DH.$$

Based on the above changes, the full deterministic model containing 8 ODEs is presented as follows,

$$\frac{dc}{dt} = J_{\text{diff}} + J_{\text{leak}} - J_{\text{serca}} + J_{\text{in}} - J_{\text{pm}}, \quad (13)$$

$$\frac{dc_b}{dt} = \gamma_1(J_{\text{IPR}} - J_{\text{diff}}), \quad (14)$$

$$\frac{dc_t}{dt} = J_{\text{in}} - J_{\text{pm}}, \quad (15)$$

$$\frac{dD}{dt} = q_{42}(1-D) - \left(\frac{q_{24}q_{62}}{q_{62} + q_{26}}\right)D, \quad (16)$$

$$\frac{dm_{24}}{dt} = \lambda_{m_{24}} \left(\frac{c_p^3}{c_p^3 + k_{24}^3} - m_{24}\right), \quad (17)$$

$$\frac{dh_{24}}{dt} = \lambda_{h_{24}} \left(\frac{k_{-24}^2}{c_p^2 + k_{-24}^2} - m_{24}\right), \quad (18)$$

$$\frac{dm_{42}}{dt} = \lambda_{m_{42}} \left(\frac{c_b^3}{c_b^3 + k_{42}^3} - m_{42}\right), \quad (19)$$

$$\frac{dh_{42}}{dt} = \lambda_{h_{42}} \left(\frac{k_{-42}^3}{c_b^3 + k_{-42}^3} - h_{42}\right), \quad (20)$$

where  $q_{24}$  and  $q_{42}$  are functions of the gating variables given by Eqs. 4 and 5. All the fluxes are the same as those of the stochastic model except  $J_{\text{IPR}} = k_{\text{IPR}}(Dq_{26}/(q_{62} + q_{26}))(c_s - c_b)$ . All the parameter values of the deterministic model are the same as those of the stochastic model and are therefore given in Tables 1 and 2.

### Reduction of the full deterministic model

The full deterministic model contains 8 variables which make the model difficult to implement and analyze. Thus, we reduce the

full model to a minimal model that still captures the crucial features of the full model. First of all,  $\lambda_{m_{42}}$ ,  $\lambda_{m_{24}}$  and  $\lambda_{h_{24}}$  are sufficiently large so that we can assume they instantaneously follow their equilibrium functions. Therefore, by taking quasi-steady state approximation to  $m_{24}$ ,  $h_{24}$  and  $m_{42}$ , we remove the three time-dependent variables from the full model.

By now, the full model has been reduced to a 5D model,

$$\frac{dc}{dt} = J_{\text{diff}} + J_{\text{leak}} - J_{\text{serca}} + J_{\text{in}} - J_{\text{pm}}, \quad (21)$$

$$\frac{dc_b}{dt} = \gamma_1(J_{\text{IPR}} - J_{\text{diff}}), \quad (22)$$

$$\frac{dc_t}{dt} = J_{\text{in}} - J_{\text{pm}}, \quad (23)$$

$$\frac{dD}{dt} = q_{42}(1-D) - \left(\frac{q_{24}q_{62}}{q_{62} + q_{26}}\right)D, \quad (24)$$

$$\frac{dh_{42}}{dt} = \lambda_{h_{42}} \left(\frac{k_{-42}^3}{c_b^3 + k_{-42}^3} - h_{42}\right). \quad (25)$$

Second, the rate of change of  $D$  approaching its equilibrium,  $\lambda_D = (q_{42}q_{62} + q_{42}q_{26} + q_{24}q_{62})/(q_{62} + q_{26})$  (calculated from Eq. 24), is at least one order larger than those of  $c$ ,  $c_t$  and  $h_{42}$ , indicating that taking the quasi-steady state approximation to Eq. 24 could not significantly affect the evolutions of  $c$ ,  $c_t$  and  $h_{42}$ . That is,

$$D = \frac{q_{42}(q_{62} + q_{26})}{q_{42}q_{62} + q_{42}q_{26} + q_{24}q_{62}}. \quad (26)$$

We emphasize here that the theory of the quasi-steady state approximation has not yet been well established, particularly about the rigorous conditions under which such a reduction is valid. Thus, our criterion of judging the validity of the reduction is checking whether the solutions of the reduced model are capable of qualitatively reproducing that of its original model. For this model, we find the reduction works. Hence, the full model is eventually reduced to a 4D model summarized as follows,

$$\frac{dc}{dt} = J_{\text{diff}} + J_{\text{leak}} - J_{\text{serca}} + J_{\text{in}} - J_{\text{pm}}, \quad (27)$$

$$\frac{dc_b}{dt} = \gamma_1(J_{\text{IPR}} - J_{\text{diff}}), \quad (28)$$

$$\frac{dc_t}{dt} = J_{\text{in}} - J_{\text{pm}}, \quad (29)$$

$$\frac{dh_{42}}{dt} = \lambda_{h_{42}} \left(\frac{k_{-42}^3}{c_b^3 + k_{-42}^3} - h_{42}\right), \quad (30)$$

where  $D$  is given by Eq. 26.



## Inclusion of calcium buffers

To check the effect of calcium buffers on oscillation frequency, we introduce a stationary buffer (no buffer diffusion), as mobile buffers are too complicated to be included in the current deterministic model. Since we have two different cytoplasmic  $\text{Ca}^{2+}$  concentrations,  $c$  and  $c_b$ , two pools of buffer with the same kinetics should be considered. Hence, the inclusion of a stationary calcium buffer is modeled by the following system,

$$\frac{dc}{dt} = J_{\text{diff}} + J_{\text{leak}} - J_{\text{serca}} + J_{\text{in}} - J_{\text{pm}} - k_+(B_t - b_1)c + k_-b_1, \quad (31)$$

$$\frac{dc_b}{dt} = \gamma_1(J_{\text{IPR}} - J_{\text{diff}}) - k_+(B_t - b_2)c_b + k_-b_2, \quad (32)$$

$$\frac{dc_t}{dt} = J_{\text{in}} - J_{\text{pm}}, \quad (33)$$

$$\frac{db_1}{dt} = k_+(B_t - b_1)c - k_-b_1, \quad (34)$$

$$\frac{db_2}{dt} = k_+(B_t - b_2)c_b - k_-b_2, \quad (35)$$

where  $b$  ( $b_1$  and  $b_2$ ) and  $B_t$  represent the concentrations of  $\text{Ca}^{2+}$ -bound buffer and total buffer respectively.  $k_+$  and  $k_-$  are the rates of  $\text{Ca}^{2+}$ -binding and  $\text{Ca}^{2+}$ -dissociation, indicating how fast the time scale of the buffer dynamics is. Fast buffer refers to the buffer with relatively large  $k_+$ . In the simulations, we use a fast buffer with  $k_+ = 100 \mu\text{M}^{-1}\cdot\text{s}^{-1}$  and  $k_- = 100 \text{s}^{-1}$  and vary  $B_t$  to test if the stochastic model and the deterministic model have a qualitatively similar  $B_t$ -dependency. Results are given in Fig. 6E.

## Numerical methods and tools for deterministic and stochastic simulations

For the stochastic model, Eqs. 1–3 and ODEs of the four gating variables in the  $\text{IP}_3\text{R}$  model are solved by the fourth-order Runge-Kutta method (RK4) and the stochastic states of  $\text{IP}_3\text{R}$  determined by the  $\text{IP}_3\text{R}$  model are solved by using a hybrid Gillespie method with adaptive timing [37]. The maximum time step size is set to be either  $10^{-4}$  s (for the 6-state  $\text{IP}_3\text{R}$  model) or  $10^{-3}$  s (for the reduced 2-state  $\text{IP}_3\text{R}$  model). All the computations are done with MATLAB (The MathWorks, Natick, MA) and the codes are provided in Supporting information (Text S1–S2). For the deterministic model, we use `ode15s`, an ODE solver in MATLAB. Accuracy is controlled by setting an absolute tolerance of  $10^{-8}$  applied to all the variables.

## References

- De Young GW, Keizer J (1992) A single-pool inositol 1, 4, 5-trisphosphate-receptor-based model for agonist-stimulated oscillations in  $\text{Ca}^{2+}$  concentration. *Proc Natl Acad Sci USA* 89: 9895–9899.
- Dupont G, Goldbeter A (1993) One-pool model for  $\text{Ca}^{2+}$  oscillations involving  $\text{Ca}^{2+}$  and inositol 1,4,5-trisphosphate as co-agonists for  $\text{Ca}^{2+}$  release. *Cell Calcium* 14: 311–322.
- Atri A, Amundson J, Clapham D, Sneyd J (1993) A single-pool model for intracellular calcium oscillations and waves in the *Xenopus laevis* oocyte. *Biophys J* 65: 1727–1739.
- Mak DOD, Pearson JE, Loong KPC, Datta S, Fernández-Mongil M, et al. (2007) Rapid ligand-regulated gating kinetics of single  $\text{IP}_3\text{R}$   $\text{Ca}^{2+}$  release channels. *EMBO Rep* 8: 1044–1051.
- Wagner LE, Yule DI (2012) Differential regulation of the  $\text{InsP}_3$  receptor type-1 and -2 single channel properties by  $\text{InsP}_3$ ,  $\text{Ca}^{2+}$  and atp. *J Physiol* 590: 3245–3259.
- Ullah G, Mak DOD, Pearson JE (2012) A data-driven model of a modal gated ion channel: the inositol 1,4,5-trisphosphate receptor in insect sf9 cells. *J Gen Physiol* 140: 159–173.
- Siekmann I, Wagner LE, Yule DI, Crampin EJ, Sneyd J (2012) A kinetic model for  $\text{IP}_3\text{R}$  type i and type ii accounting for mode changes. *Biophys J* 103: 658–668.
- Cao P, Donovan G, Falcke M, Sneyd J (2013) A stochastic model of calcium puffs based on single-channel data. *Biophys J* 105: 1133–1142.
- Smith IF, Parker I (2009) Imaging the quantal substructure of single  $\text{IP}_3\text{R}$  channel activity during  $\text{Ca}^{2+}$  puffs in intact mammalian cells. *Proc Natl Acad Sci USA* 106: 6404–6409.

## Statistical analysis

Data analysis is performed on the  $\text{Ca}^{2+}$  traces with relatively stable baselines and less noise. A moving average of every 3 data points is used to improve the data by smoothing out short-term fluctuations (Fig. 2A is an improved result). Due to large variations in baseline, amplitude, and level of noise in data, we used two thresholds to get samples: a low threshold, 20% of the amplitude of the largest spike above the baseline, to initially filter baseline noise out; and a relatively high threshold, 50% of the amplitude of the largest spike above the baseline, to further remove small spikes that cannot initiate waves. For simulated stochastic traces of variable  $c$ , we first convert it to fluorescence ratio ( $F/F_0$ ) by using  $F/F_0 = c(c_0 + K_d)/(c_0c + c_0K_d)$  where the dissociation constant of Oregon Green  $K_d = 0.17 \mu\text{M}$  and resting  $[\text{Ca}^{2+}]_i$ ,  $c_0 = 0.1 \mu\text{M}$ . We then used the same sampling procedure mentioned above to obtain samples. After samples are chosen, ISIs and spike durations are calculated based on the low threshold. Simulated traces used to calculate average frequency are about 200–400 seconds long. All the samplings and linear least-squares fittings are implemented using MATLAB (see Text S3–S4 for Matlab codes).

## Supporting Information

**Dataset S1 ASMC calcium fluorescence trace data.** The data files are in Excel format and compressed in a zip file. Each Excel file has a name showing their information. For example, “S2\_SMC6\_MCh200nM” means data are from ASMC No. 6 in lung slice No. 2 by using 200 nM MCh. In each file, there are four columns which represent (from left to right) time(s), fluorescence intensity,  $F/F_0$  and average  $F/F_0$ . (ZIP)

**Text S1 Matlab code for simulation using 6 state  $\text{IP}_3\text{R}$  model.** (DOCX)

**Text S2 Matlab code for simulation using 2 state  $\text{IP}_3\text{R}$  model.** (DOCX)

**Text S3 Matlab code for experimental data analysis.** (DOCX)

**Text S4 Matlab code for simulation analysis.** (DOCX)

## Acknowledgments

We acknowledge many useful conversations with Martin Falcke.

## Author Contributions

Conceived and designed the experiments: JS GD MJS. Performed the experiments: XT. Analyzed the data: PC. Contributed to the writing of the manuscript: PC JS. Conceived and designed the model: PC JS GD. Performed the simulations: PC.

10. Brumen M, Fajmut A, Dobovišek A, Roux E (2005) Mathematical modelling of  $\text{Ca}^{2+}$  oscillations in airway smooth muscle cells. *J Biol Phys* 31: 515–524.
11. Sneyd J, Tsaneva-Atanasova K, Reznikov V, Bai Y, Sanderson MJ, et al. (2006) A method for determining the dependence of calcium oscillations on inositol trisphosphate oscillations. *Proc Natl Acad Sci USA* 103: 1675–1680.
12. Wang IY, Bai Y, Sanderson MJ, Sneyd J (2010) A mathematical analysis of agonist- and kcl-induced  $\text{Ca}^{2+}$  oscillations in mouse airway smooth muscle cells. *Biophys J* 98: 1170–1181.
13. Croisier H, Tan X, Perez-Zoghbi JF, Sanderson MJ, Sneyd J, et al. (2013) Activation of store-operated calcium entry in airway smooth muscle cells: insight from a mathematical model. *PLoS ONE* 8(7): e69598 doi:10.1371/journal.pone.0069598.
14. Marchant JS, Parker I (2001) Role of elementary  $\text{Ca}^{2+}$  puffs in generating repetitive  $\text{Ca}^{2+}$  oscillations. *EMBO J* 20: 65–76.
15. Skupin A, Kettenmann H, Winkler U, Wartenberg M, Sauer H, et al. (2008) How does intracellular  $\text{Ca}^{2+}$  oscillate: by chance or by the clock? *Biophys J* 94: 2404–2411.
16. Perez JF, Sanderson MJ (2005) The frequency of calcium oscillations induced by 5-ht, ach, and kcl determine the contraction of smooth muscle cells of intrapulmonary bronchioles. *J Gen Physiol* 125: 535–553.
17. Bai Y, Edelmann M, Sanderson MJ (2009) The contribution of inositol 1,4,5-trisphosphate and ryanodine receptors to agonist-induced  $\text{Ca}^{2+}$  signaling of airway smooth muscle cells. *Am J Physiol Lung Cell Mol Physiol* 297: L347–L361.
18. Bird GSJ, Putney JW (2005) Capacitative calcium entry supports calcium oscillations in human embryonic kidney cells. *J Physiol* 562(3): 697–706.
19. Sneyd J, Tsaneva-Atanasova K, Yule DI, Thompson JL, Shuttleworth TJ (2004) Control of calcium oscillations by membrane fluxes. *Proc Natl Acad Sci USA* 101: 1392–1396.
20. Mahn K, Hirst SJ, Ying S, Holt MR, Lavender P, et al. (2009) Diminished sarco/endoplasmic reticulum  $\text{Ca}^{2+}$  atpase (serca) expression contributes to airway remodelling in bronchial asthma. *Proc Natl Acad Sci USA* 106: 10775–10780.
21. Sathish V, Leblebici F, Kip SN, Thompson MA, Pabelick CM, et al. (2008) Regulation of sarcoplasmic reticulum  $\text{Ca}^{2+}$  reuptake in porcine airway smooth muscle. *Am J Physiol Lung Cell Mol Physiol* 294: L787–L796.
22. Zeller S, Rüdiger S, Engel H, Sneyd J, Warnecke G, et al. (2009) Modeling of the modulation by buffers of  $\text{Ca}^{2+}$  release through clusters of  $\text{IP}_3$  receptors. *Biophys J* 97: 992–1002.
23. Li Y, Rinzel J (1994) Equations for  $\text{InsP}_3$  receptor-mediated  $[\text{Ca}^{2+}]_i$  oscillations derived from a detailed kinetic model: a hodgkin-huxley like formalism. *J Theor Biol* 166: 461–473.
24. Keener J, Sneyd J (2009) *Mathematical Physiology*, Second Edition. Springer, New York.
25. Ionescu L, White C, Cheung KH, Shuai J, Parker I, et al. (2007) Mode switching is the major mechanism of ligand regulation of  $\text{InsP}_3$  receptor calcium release channels. *J Gen Physiol* 130: 631–645.
26. Shuai JW, Jung P (2002) Stochastic properties of  $\text{Ca}^{2+}$  release of inositol 1,4,5-trisphosphate receptor clusters. *Biophys J* 83: 87–97.
27. Dupont G, Abou-Loergne A, Combettes L (2008) Stochastic aspects of oscillatory  $\text{Ca}^{2+}$  dynamics in hepatocytes. *Biophys J* 95: 2193–2202.
28. Kannan MS, Prakash YS, Brenner T, Mickelson JR, Sieck GC (1997) Role of ryanodine receptor channels in  $\text{Ca}^{2+}$  oscillations of porcine tracheal smooth muscle. *Am J Physiol* 272: L659–L664.
29. Tazzeo T, Zhang Y, Keshavjee S, Janssen LJ (2008) Ryanodine receptors decant internal  $\text{Ca}^{2+}$  store in human and bovine airway smooth muscle. *Eur Respir J* 32: 275–284.
30. Rössmeyer AR, Bai Y, Delmotte P, Uy KF, Thistlethwaite P, et al. (2010) Human airway contraction and formoterol-induced relaxation is determined by  $\text{Ca}^{2+}$  oscillations and  $\text{Ca}^{2+}$  sensitivity. *Am J Respir Cell Mol Biol* 43: 179–191.
31. Soeller C, Cannell MB (2004) Analysing cardiac excitation-contraction coupling with mathematical models of local control. *Prog Biophys Mol Biol* 85: 141–162.
32. Thurley K, Skupin A, Thul R, Falcke M (2012) Fundamental properties of  $\text{Ca}^{2+}$  signals. *Biochim Biophys Acta* 1820(8): 1185–1194.
33. Dickinson G, Parker I (2013) Factors determining the recruitment of inositol trisphosphate receptor channels during calcium puffs. *Biophys J* 105: 2474–2484.
34. Rüdiger S, Shuai JW, Sokolov IM (2010) Law of mass action, detailed balance, and the modeling of calcium puffs. *Phys Rev Lett* 105(4): 048103 doi:10.1103/PhysRevLett.105.048103.
35. Rüdiger S, Jung P, Shuai J (2012) Termination of  $\text{Ca}^{2+}$  release for clustered  $\text{IP}_3\text{R}$  channels. *PLoS Comput Biol* 8(5): e1002485 doi:10.1371/journal.pcbi.1002485.
36. Chandrasekera PC, Kargacim ME, Deans JP, Lytton J (2009) Determination of apparent calcium affinity for endogenously expressed human sarco(endoplasmic reticulum calcium-atpase isoform serca3. *Am J Physiol Cell Physiol* 296: C1105–C1114.
37. Rüdiger S, Shuai JW, Huisinga W, Nagaiah C, Warnecke G, et al. (2007) Hybrid stochastic and deterministic simulations of calcium blips. *Biophys J* 93: 1847–1857.